HanGrawler: Large-Payload and High-Speed Ceiling Mobile Robot Using Crawler

Rui Fukui , *Member, IEEE*, Yudai Yamada , *Student Member, IEEE*, Keisuke Mitsudome, Katsuya Sano, and Shin'ichi Warisawa

Abstract—In this article, we present a ceiling-mounted mobile robot, HanGrawler, with high-speed mobility and the ability to freely select and adjust its route under a ceiling plate. HanGrawler hangs from the holes of a perforated metal ceiling plate using newly developed mechanically constrained hanging mechanisms mounted on crawler-type traveling equipment. These mechanisms continuously grasp the ceiling holes while moving in a straight line. Specially designed turntables are installed at certain ceiling points to change the HanGrawler movement direction to facilitate two-dimensional motion. A performance evaluation experiment confirms that HanGrawler can travel linearly at 0.1 m/s, turn at an 8.5°/s rotational speed, and carry a maximum load of 60 kg. The experiment also reveals that HanGrawler can carry a heavy load only when the timings of the hanging mechanism hooking motions and turntable rotational speed are tuned. This transport system can be utilized not only for part transportation on production lines but also for logistics in general.

Index Terms—Ceiling mobile robot, logistics, mechanical hanging mechanism design, perforated metal.

I. INTRODUCTION

AUTOMATIC guided vehicles (AGVs) are utilized at production sites [1], [2]. AGV transport routes can be changed easily and these vehicles are suitable for use in factories producing small quantities of various models. However, AGV transport routes interfere with worker and production facility spaces; this can be avoided and greater transport route freedom can be achieved by establishing AGV motion on the ceilings. At present, AGV ceiling movement requires a rail, while transport route adjustment necessitates rail replacement. Such AGVs are unsuitable for automobile assembly factories, etc., in which production lines are changed frequently.

Rui Fukui, Yudai Yamada, Keisuke Mitsudome, and Shin'ichi Warisawa are with the Department of Human and Engineered Environmental Studies, The University of Tokyo, Chiba 277-8563, Japan (e-mail: fukui@edu.k.u-tokyo.ac.jp; yamadayudai@lelab.t.u-tokyo.ac.jp; mitsudomekeisuke@lelab.t.u-tokyo.ac.jp; warisawa@edu.k.u-tokyo.ac.jp).

Katsuya Sano was with the Department of Mechanical Engineering, The University of Tokyo, Tokyo 113-8656, Japan. He is now with Kawasaki Heavy Industries Motorcycle and Engine Company, Kawasaki Heavy Industries, Ltd., Tokyo 105-8315, Japan (e-mail: sano@hnl.t.u-tokyo.ac.jp).

There are two approaches to route adjustment for a ceiling-mounted mobile robot—development of: a) a robot with 2-D ceiling movement and b) easy rail replacement for a rail-type robot. Herein, approach a) is discussed, because the operation suspension period during route adjustment can be reduced. To date, 2-D-motion ceiling-mobile and wall-climbing robots have been investigated for application to disaster relief and cleaning. Five ceiling- and wall-attachment methods have been considered, using the following:
1) vacuum suction [3]–[11];
2) electromagnets [12]–[14];
3) permanent magnets [15]–[20];
4) mechanical constraints [21]–[27];
5) adhesive, van der Waals', and electrostatic forces [28]–[33].

In the mechanical-constraint method, attachments are used for hanging from ceiling holes or wall protrusions. For both the permanent-magnet and mechanical-constraint techniques, the attachment force to the ceiling can be increased easily and these techniques can be used during blackouts. Herein, mechanical constraint is considered because lighter and more compact attachments can be designed than those that are typically used with the permanent-magnet approach. The mechanical-constraint method takes the following three approaches: 1) bionic spine for flat ceilings and walls [21]–[23]; 2) grabbing mechanism for protruding structures [24], [25]; and 3) hanging mechanism for perforated structures [26], [27]. Approach 1) uses legs or wheels equipped with small spines that can attach to tiny protrusions on a ceiling or wall. However, this approach is not suitable for heavy-object transportation because the small spines have low durability. In approach 2), a robot moves on rails or climbs protrusions fixed to a wall. This approach involves the complicated installation of ceiling rails or protrusions and cannot realize easy route adjustment. In approach 3), a robot hangs from the holes in a perforated ceiling plate using mechanical hanging mechanisms. In previous studies, robots have successfully carried 24- and 35-kg loads, so this approach is regarded as being the most suitable for heavy-object transportation.

In our previous work, HangBot [27] was presented. HangBot mechanically hangs from a perforated metal ceiling plate and moves in two dimensions. However, HangBot has two separate body parts and moves intermittently (like an inchworm) at 0.03 m/s, which is critically slower than general conveying machines. In contrast, Rise-Rover [10], an alternative design using a high-speed crawler mechanism moves at 0.5 m/s, more than
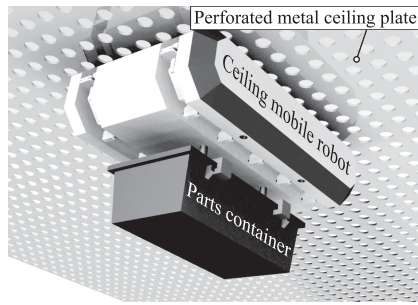
Fig. 1. Conceptual sketch of ceiling mobile robot.

Fig. 2. Configuration of HanGrawler ceiling mobile robot.

Fig. 3. Hanging mechanisms on roller can lock onto one ceiling hole only.

ten times faster than HangBot. However, Rise-Rover utilizes vacuum-suction attachment and, thus, heavy-object transport across a ceiling is difficult.

In this study, we develop a ceiling mobile robot named "HanGrawler," with easy transport route adjustment, 2-D movement, a 50-kg payload, and 0.1-m/s speed using a crawler mechanism. As continuous movement is essential to attain high speed, a combined mechanical-constraint and continuous-movement mechanism is employed. The payload conforms to the HEADS Co. AGV specifications [34]. The transport speed conforms to the speed of an automobile factory line. That is, when producing 10 000 cars per month, production of one car requires 57.5 s [35]. Assuming 3.5-m automobile body length, 6-m intercar spacing, and 60-s production time for one car, the line speed of the final assembly process is 6/60 = 0.1 m/s.

The contributions of this study are a discussion and solution of the technological problems associated with such a novel robot. This article is structured as follows. In Section II, the continuous-movement method and the problems affecting the selected crawler, hanging, and turning mechanisms are discussed, along with their solutions. In Section III, the above-mentioned mechanism designs and HanGrawler implementation are presented. Section IV describes a performance-evaluation experiment, in which the target performance is achieved via the proposed attachment and movement methods. Section V concludes this article.

II. CRAWLER MECHANISM FOR REALIZING HIGH-SPEED MOVEMENT UNDER CEILING PLATE

A. Continuous-Movement Method

Fig. 1 is a conceptual sketch of the target ceiling mobile robot performing parts transportation. Fig. 2 shows the HanGrawler configuration. Hanging mechanisms for mechanical attachment to the ceiling plate are mounted on the crawler mechanism, and HanGrawler achieves continuous movement by locking onto and releasing from the ceiling plate using the hanging mechanism.

To achieve continuous movement, the robot must use a mechanism that achieves both contact and fixing between the hanging mechanisms and ceiling plate, such as a roller or crawler. If the hanging mechanisms are mounted on the circumference of a roller, the adjacent hanging mechanisms cannot lock onto the holes because there is only one contact point or line (see Fig. 3). Therefore, multiple rollers are necessary for stable attachment.
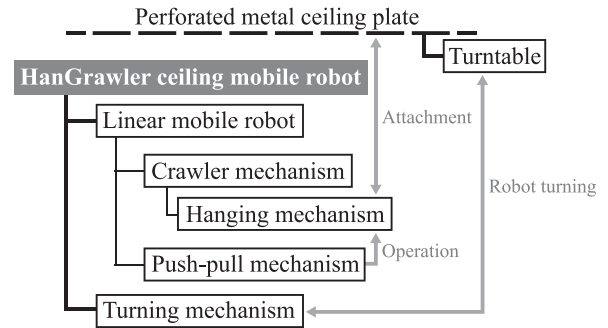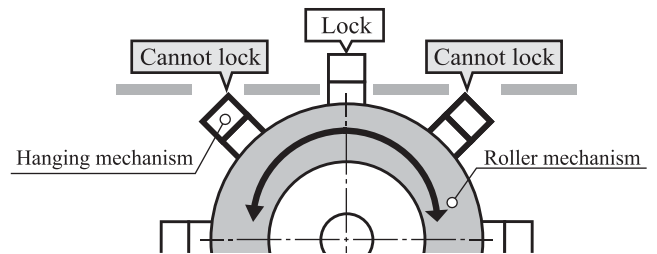
However, if multiple rollers are installed, the robot configuration becomes complex, because the robot must synchronize the rotation of multiple rollers and the hanging-mechanism locking/release motions. In contrast, for hanging mechanisms mounted on the circumference of a crawler mechanism, the robot can lock onto multiple ceiling-plate holes because the crawler establishes plane contact with the ceiling plate. Thus, the robot can switch between multiple hanging mechanisms during movement without synchronizing multiple mechanisms, because the crawler mechanism is a unitary structure. Thus, a crawler mechanism was used in this study. To the best of our knowledge, a ceiling mobile robot combining hanging and crawler mechanisms has not been reported to date. In the following subsections, the problems and solutions associated with this combination are discussed. Problems 1 and 3 are derived from the critical disadvantages of the HangBot for realizing high-speed and heavy-object transportation. Problem 2 is a new design assignment for realizing practical and stable crawler motion. Problem 4 is an inevitable problem of the crawler mechanism that is suitable for straight motion but unsuitable for curved motion and rotation.

B. Problem 1: Lock and Release State Switching for Zero Load on Hanging Mechanism

The ceiling mobile robot moves by repeating the following two actions: 1) a hanging mechanism is inserted into and locks onto a ceiling hole and 2) a hanging mechanism is released and extracted from a ceiling hole. If a large load is applied to a given hanging mechanism, the force required for locking and release increases and the actuator for state switching becomes quite large, preventing high-speed movement. To remove the load
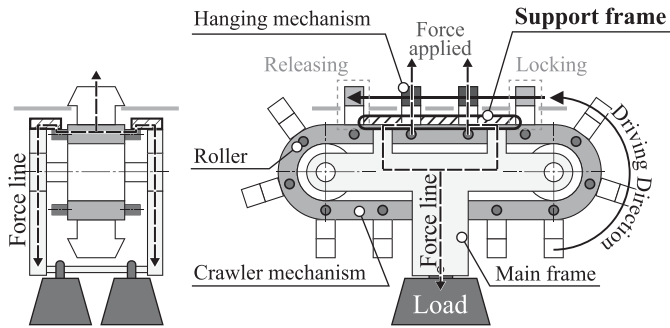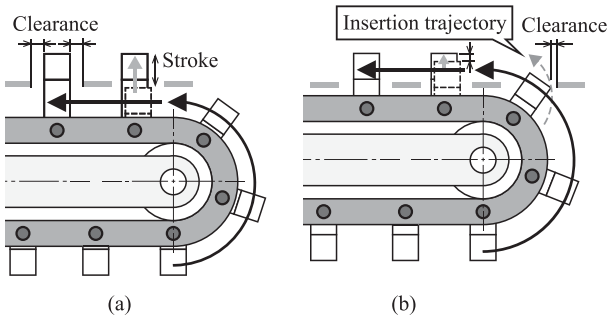
Fig. 4.   Conceptual sketch of support frame.

Fig. 5.   Hanging-mechanism trajectory.

Fig. 6.   Linear mobile robot cannot change travel direction without assistance.

from the hanging mechanism during switching, the robot applies the load to hanging mechanisms other than the switching target. To realize this behavior, we positioned a support frame between the ceiling and crawler mechanism, as shown in Fig. 4. The robot consists of a main frame and a crawler mechanism. The crawler mechanism operates between the main frame and the support frame and holds the inserted hanging mechanisms. This support frame is connected to the main frame, which supports the transport load. The support frame is in contact with rollers installed on the crawler mechanism. When a load is applied to the robot (see Fig. 4), the load force line (dashed line) passes through the rollers immediately below the support frame and the hanging mechanisms (filled in black) connected to these rollers only. This means that the load is not applied to the operation target hanging mechanisms (filled in gray) during switching.

C. Problem 2: Prevention of Interference Between Trajectories of Hanging Mechanism and Ceiling Hole

There are two hanging-mechanism insertion methods (see Fig. 5): a) vertical insertion into the ceiling plate and b) insertion into the ceiling plate along with the sprocket or guide roller. In method a), a clearance gap between the hanging mechanism and ceiling hole can be secured easily. The crawler mechanism can insert the hanging mechanism when the ceiling hole is wider than the hanging mechanism. However, because the stroke of the hanging mechanism and the actuator for locking and release become long, the mechanism becomes bulky and the time required for insertion and extraction increases. In method b), the hanging mechanism is inserted by the robot movement.
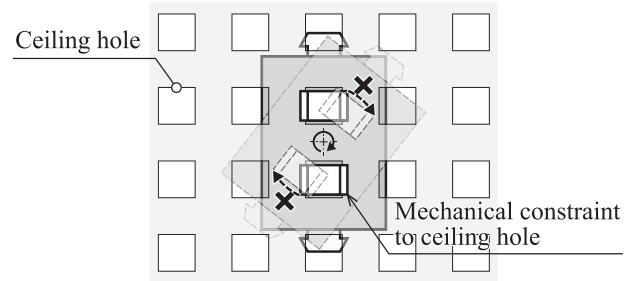
Thus, the hanging mechanism stroke and the actuator for locking and release become short, and the time required for insertion and extraction decreases. However, because the radius of the hanging-mechanism trajectory is slightly larger than that of the crawler mechanism, and because the clearance gap with the ceiling hole is small, great care must be taken in the design phase to avoid interference between the hanging mechanism and ceiling hole. In this work, method b) was adopted because it was expected to contribute to robot movement acceleration. In Section III-A, the trajectory variation of the ceiling-hole edge (from the hanging mechanism perspective) depending on the crawler guide structure shape is analyzed, and an appropriate hanging-mechanism insertion trajectory that prevents interference with the ceiling hole and achieves compactness is presented.

D. Problem 3: High-Speed State Switching of Hanging Mechanisms

A hanging mechanism locks onto and releases a ceiling hole under crawler-mechanism driving. If the time required for switching between lock and release states is long, the switching time becomes a robot movement bottleneck that decreases the movement speed. For acceleration, high-speed hanging-mechanism state switching is necessary. To satisfy this requirement, a one-action process is used for the HanGrawler lock-and-release hanging-mechanism state switching. Details of the design are presented in Section III-B. Further, if an actuator for lock and release is mounted on each hanging mechanism, a large number of actuators are necessary. Therefore, lock and release should be performed by a small number of actuators mounted on the robot body or by passive guide structures.

Solving Problems 1, 2, and 3 allows the ceiling mobile robot to attach to the ceiling via the hanging mechanisms, and to achieve linear movement via the crawler mechanism.

E. Problem 4: Change of Travel Direction for 2-D Movement

To realize 2-D movement for the ceiling mobile robot, travel direction change by the linear mobile robot is necessary. Thus, part of the crawler mechanism must be able to skid across the ceiling plate. However, this is prevented by the hanging mechanism being mechanically constrained to the ceiling holes (see Fig. 6). Therefore, a direction-change mechanism for the linear mobile robot is necessary. Considering the robot deployment and
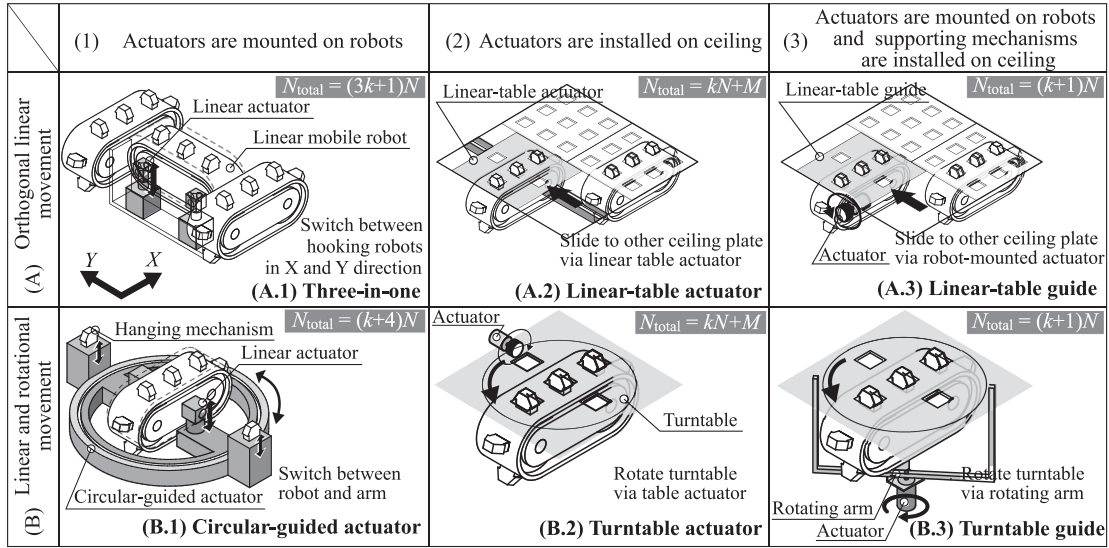
Fig. 7. Direction-change mechanism candidates. N_{total} is the total number of actuators in the expected transport system, k is the number of actuators in one linear mobile robot, N is the number of robots, and M is the number of positions for direction changing.

the direction-change mechanism at the actual production site, the number of actuators used in the expected transport system should be small to reduce the required amount of maintenance steps. In addition, transport route variation every few years can be expected.

In total six direction-change methods are compared here (see Fig. 7), being evaluated based on the number of actuators and ease of transport route adjustment. There are the following two methods of 2-D movement:

A) orthogonal linear movement;
B) linear and rotational movement.

There are the following three actuator mounting methods:
1) actuators are mounted on robots;
2) actuators are installed on ceiling;
3) actuators are mounted on robots and supporting mechanisms are installed on ceiling.

Thus, there are $2 \times 3 = 6$ possible combinations for the direction-change mechanism. Hereafter, N_{total} is the total number of actuators in the expected transport system, k is the number of actuators in one linear mobile robot, N is the number of robots, and M is the number of positions for direction change and is considered only in method 2), where the actuators are installed on the ceiling.

A.1) The three-in-one method realizes 2-D motion with a combination of three linear mobile robots and switching between hooking robots in the X- and Y- directions. $N_{\text{total}} = (3\,k+1)N$, because one actuator is needed for switching.

B.1) The circular-guided actuator method involves a circular-guided actuator with hanging mechanisms for ceiling-plate locking. Rotation occurs through switching between the circular-guided actuator and a linear mobile robot. One, two, and one actuators are needed for the circular-guided actuator, its locking, and switching, respectively; thus, $N_{\text{total}} = (k+1+2+1)$ $N = (k+4)N$.

TABLE I
COMPARISON OF ACTUATOR NUMBERS AND TWO CORE SPECIFICATIONS OF DIRECTION-CHANGE MECHANISM CANDIDATES

$k = 3$	N_{total}					
Number of N, M	(A.1) $(3k+1)N$	(B.1) $(k+4)N$	(A.2) $kN+M$	(B.2) $kN+M$	(A.3) $(k+1)N$	(B.3) $(k+1)N$
N = M = 1	10	7	4	4	4	4
N = M = 10	100	70	40	40	40	40
N = M = 100	1000	700	400	400	400	400
Efficient waiting time	✓	✓	✗	✓	✗	✓
Easy transport route adjustment	✓	✓	✗	✗	✗	✓

A.2) The linear-table actuator method involves a linear-table actuator on a ceiling plate. The actuator slides the robot to other ceiling plates. $N_{\text{total}} = kN + 1$.

B.2) The turntable actuator method involves a turntable on a ceiling plate. A ceiling-installed actuator rotates the turntable and robot. $N_{\text{total}} = kN + M$.

A.3) The linear-table guide method features a linear-table guide on a ceiling plate. A robot-mounted actuator slides the robot to other ceiling plates. $N_{\text{total}} = (k+1)N$.

B.3) The turntable guide method involves a turntable on a ceiling plate. A robot-mounted actuator rotates the turntable and robot. $N_{\text{total}} = (k+1)N$.

Table I compares N_{total} for the above-mentioned six methods. Assuming that a linear mobile robot needs one actuator for a linear movement to drive a crawler mechanism and two actuators for hanging-mechanism locking and release, as described in Section II-D, $k = 3$ was adopted in this study. Methods A.1) and B.1) need many robot-mounted actuators and there are relatively many actuators in the system. Methods A.2) and A.3) may involve long wait times. The actuator number is
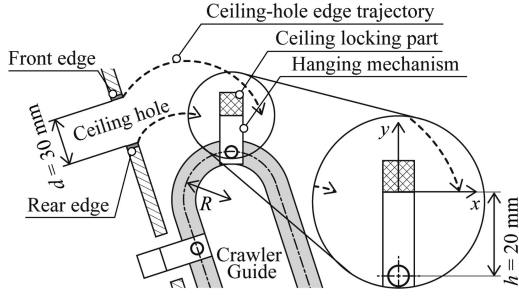
Fig. 8. Ceiling-hole edge trajectories from hanging-mechanism perspective.

Fig. 9. Schematic diagram of Fig. 8.

expected to be acceptable for both B.2) and B.3). However, electric equipment adjustment with transport route variation is necessary for B.2); thus, the "easy transport route adjustment" requirement is not satisfied. Hence, B.3) was adopted in this study, having an acceptable actuator number and satisfying the two core specifications.

III. CEILING MOBILE ROBOT DESIGN

A. Design of Hanging-Mechanism Trajectory With Ceiling-Hole Insertion

HanGrawler is an innovative ceiling mobile robot combining hanging and crawler mechanisms. Therefore, a new design method for the hanging-mechanism trajectory was developed. When the crawler mechanism inserts the hanging mechanism into a ceiling hole, adjustment of the hanging-mechanism position and posture relative to the ceiling hole is necessary to prevent ceiling-hole interference.

When the hanging mechanism has locked onto the ceiling hole, a relative position is established between both, into which the crawler mechanism is inserted. Therefore, registration of the hanging mechanism to the ceiling hole is unnecessary. Thus, we considered adjusting the hanging-mechanism posture.

To prevent interference between the hanging mechanism and ceiling hole, the trajectory of the ceiling-hole edge from the hanging-mechanism perspective (see Fig. 8) is significant. (x, y) are the coordinates of the ceiling-hole edge trajectory. The crawler and hanging mechanisms move along a crawler guide with the radius R. Hereafter, the hanging-mechanism part protruding toward the ceiling upper side is called the "ceiling locking part." During ceiling-hole insertion, the edge trajectory is determined by the ceiling-hole size and the trajectory of the ceiling locking part. We set the ceiling-hole width $d = 30$ mm with reference to HangBot [27]. The distance between the crawler center line and ceiling locking part $h = 20$ mm, based on d.

First, we considered a circular guide having the simplest trajectory. We derived the ceiling-hole edge trajectory from the hanging-mechanism perspective during insertion for circular guides with radius $R = 50, 100,$ and 200 mm (see Fig. 9). The maximum R (200 mm) is defined by considering the height of the robot body. We considered the trajectory of the ceiling-hole edge points P_{rear} and P_{front} relative to the coordinate system (x', y') with the origin at the guide center, when the hanging-mechanism angle was $0 \leq \phi \leq \pi/2$.
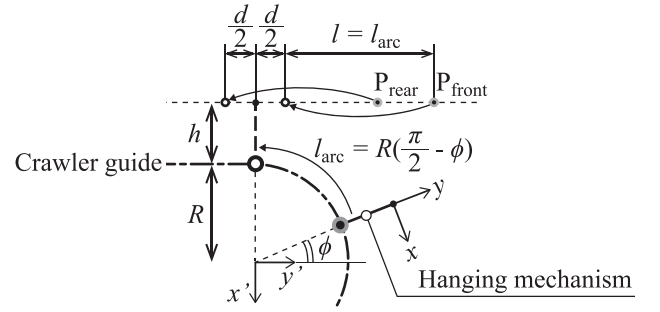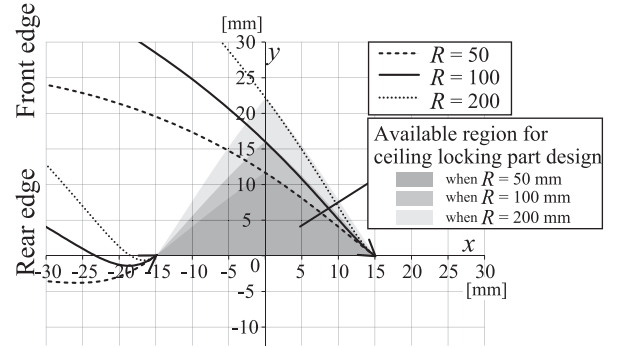

Fig. 10. Ceiling-hole edge trajectories for circular arc-shaped guide.

The designed robot moves on the ceiling while inserting the hanging mechanism and moving the crawler mechanism. Therefore, the hanging-mechanism movement distance l_{arc} is equal to that from the ceiling hole l. The coordinates of $P_{\text{rear}}(x'_{\text{rear}}, y'_{\text{rear}})$ and P_{front} are defined as

$$\begin{cases} x'_{\text{rear}} = -R - h \\ y'_{\text{rear}}(\phi) = R(\frac{\pi}{2} - \phi) - \frac{d}{2}, \ 0 \leq \phi \leq \frac{\pi}{2} \end{cases} \quad (1)$$

$$\begin{cases} x'_{\text{front}} = -R - h \\ y'_{\text{front}}(\phi) = R(\frac{\pi}{2} - \phi) + \frac{d}{2}, \ 0 \leq \phi \leq \frac{\pi}{2} \end{cases} \quad (2)$$

respectively. In these equations, the position of the hanging mechanism having moved from $\phi = 0$ to $\pi/2$ is set to be the center of the ceiling hole, so that $y'_{\text{rear}}(\pi/2) = -d/2, y'_{\text{front}}(\pi/2) = d/2$. The coordinate system of the hanging-mechanism center $\{x, y\}$ is established by rotating and translating the coordinate system of the guide center $\{x', y'\}$. Therefore, using the rotation matrix

$$\Theta(\alpha) = \begin{pmatrix} \cos\alpha & \sin\alpha \\ -\sin\alpha & \cos\alpha \end{pmatrix} \quad (3)$$

the coordinates of P_{rear} and P_{front} are

$$\begin{pmatrix} x_{\text{i}}(\phi) \\ y_{\text{i}}(\phi) \end{pmatrix} = \Theta(\phi) \begin{pmatrix} x'_{\text{i}} \\ y'_{\text{i}}(\phi) \end{pmatrix} + \begin{pmatrix} 0 \\ -R - h \end{pmatrix}, (\text{i} = \text{rear}, \text{front}). \quad (4)$$

Fig. 10 shows the trajectory of the ceiling-hole edge for guides with $R = 50, 100,$ and 200 mm derived from (4). As the robot moves similarly forward and backward, this trajectory exists symmetrical to the y-axis. The available regions for the ceiling locking part are colored in gray in the figure. The areas of
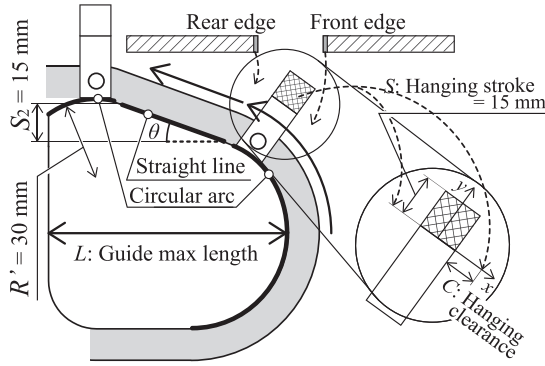
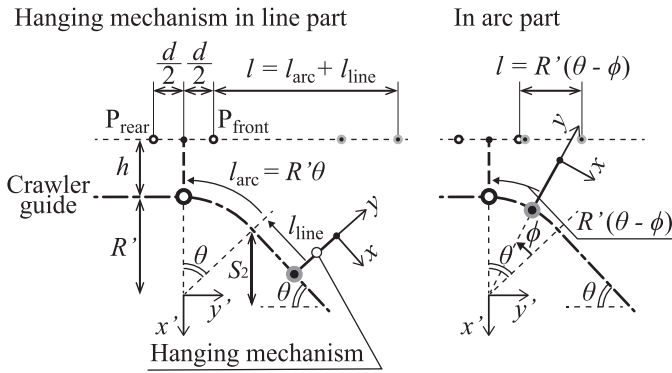Fig. 11. Overview of straight-line and circular-arc-shaped guide.

Fig. 12. Schematic diagram of Fig. 11.

each region are approximately 180, 240, and 330 mm^2 when $R = 50, 100,$ and 200, respectively. When R increases, the area increases, and it is easier to design the ceiling locking part. However, as a locking and release mechanism is built into the hanging mechanism, this region seems to constitute a large restriction on the hanging-mechanism design, because it is difficult for such triangles to contain a mechanism.

Thus, we aimed to secure a substantially large region for the hanging mechanism using a guide shape combining a straight line and a circular arc (see Fig. 11). In this approach, the hanging mechanism is inserted into the ceiling hole along with the upper circular arc part of the guide after passing the straight line part. The hanging-mechanism trajectory is designed to adjust the angle of the straight line θ. The available region for the ceiling locking part can be expanded by reducing the radius of the upper circular arc of the guide R', as shown in Fig. 10. Based on h, R' was set to 30 mm, and the height of the straight line S_2 was set to 15 mm.

We considered the trajectory of P_{rear} and P_{front} from the guide-center coordinate system $\{x', y'\}$ perspective (see Fig. 12). The hanging mechanism moves along l_{line} and then, l_{arc}. Therefore, the movement distance $l_{\text{line}} + l_{\text{arc}}$ is equal to the distance from the ceiling hole l. The straight line angle is θ, so that the angle of l_{arc} is also θ and $l_{\text{arc}} = R'\theta$. When the hanging mechanism moves linearly, the coordinates of P_{rear} are

$$\begin{cases} x'_{\text{rear}} = -R' - h \\ y'_{\text{rear}}(l_{\text{line}}) = R'\theta + l_{\text{line}} - \frac{d}{2}, \ 0 \le l_{\text{line}} \le \frac{S_2}{\sin\theta} \end{cases} \quad (5)$$
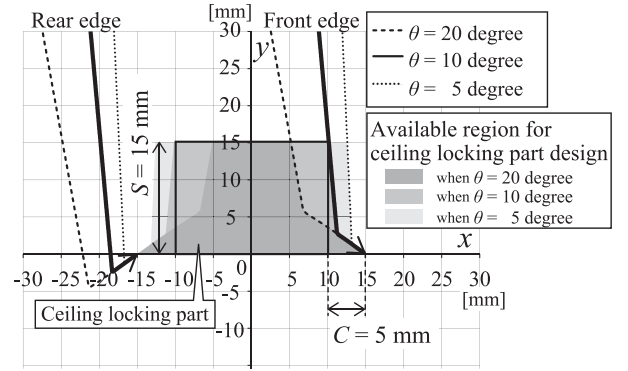

Fig. 13. Ceiling-hole edge trajectories for guide with straight line and circular arc shape.

where l_{line} is the distance to the circular arc part. The coordinates of P_{front} are

$$\begin{cases} x'_{\text{front}} = -R' - h \\ y'_{\text{front}}(l_{\text{line}}) = R'\theta + l_{\text{line}} + \frac{d}{2}, \ 0 \le l_{\text{line}} \le \frac{S_2}{\sin\theta} \end{cases} \quad (6)$$

Through a similar transformation as that for (4), the coordinates of P_{rear} and P_{front} become

$$\begin{pmatrix} x_i(\phi) \\ y_i(\phi) \end{pmatrix} = \Theta\left(\frac{\pi}{2} - \theta\right)\begin{pmatrix} x'_i \\ y'_i(l_{\text{line}}) \end{pmatrix} + \begin{pmatrix} -l_{\text{line}} \\ -R - h \end{pmatrix},$$
$$(i = \text{rear}, \text{front}). \quad (7)$$

When the hanging mechanism is moving according to the circular arc, the remaining length l is $R'(\theta - \phi)$. The coordinates of P_{rear} and P_{front} are

$$\begin{cases} x'_{\text{rear}} = -R' - h \\ y'_{\text{rear}}(\phi) = R'(\theta - \phi) - \frac{d}{2}, \ 0 \le \phi \le \theta \end{cases} \quad (8)$$

$$\begin{cases} x'_{\text{front}} = -R' - h \\ y'_{\text{front}}(\phi) = R'(\theta - \phi) + \frac{d}{2}, \ 0 \le \phi \le \theta \end{cases} \quad (9)$$

respectively. Through transformation, the coordinates of P_{rear} and P_{front} become

$$\begin{pmatrix} x_i(\phi) \\ y_i(\phi) \end{pmatrix} = \Theta\left(\frac{\pi}{2} - \theta + \phi\right)\begin{pmatrix} x'_i \\ y'_i(\phi) \end{pmatrix} + \begin{pmatrix} 0 \\ -R - h \end{pmatrix},$$
$$(i = \text{rear}, \text{front}). \quad (10)$$

Fig. 13 shows the ceiling-hole edge trajectories for guides with $\theta = 5°, 10°,$ and $20°$ derived from (7) and (10). For the case where the length of the part above the ceiling in the y-axis direction S, i.e., the hanging-mechanism hanging stroke, is set to 15 mm, the available region for the ceiling locking part is colored in gray (see Fig. 13). The areas of each region are approximately 390, 330, and 230 mm^2 in $\theta = 5, 10,$ and 20, respectively. For $\theta = 5$ and 10, the available regions are larger than the circular arc guide. For $S = 15$ mm, when S_2 is less than 15 mm, the hanging mechanism interferes with the ceiling at the circular arc before the straight line. Hence, we set $S_2 = 15$ mm and the full length of guide L became approximately 300 and 200 mm in $\theta = 5°$ and 10°, respectively. Considering the AGV size [34] to determine the target performance, we set the ceiling mobile
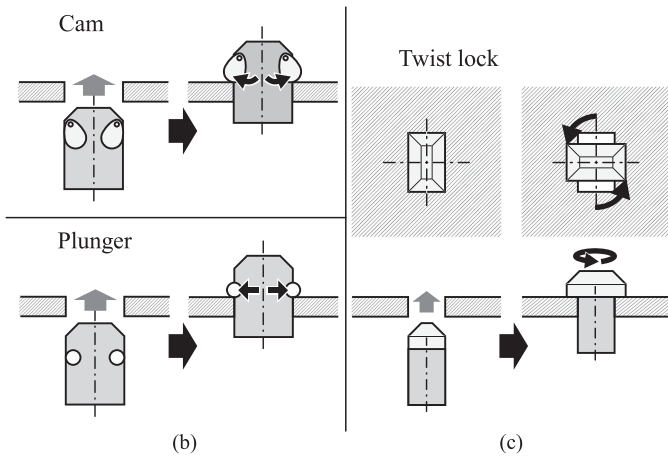
Fig. 14.   Conceptual sketches of lock mechanisms.

robot size to 1 m or less and L to 250 mm or less. Therefore, we adopted a guide combining a circular arc and a straight line with $\theta = 10°$. Further, R was set according to the full length of the robot because R does not affect the size of the available region. For $S = 15$ mm, the available region is $-10 \leq x \leq 10$, as shown in Fig. 13. A minimum clearance gap C of 5 mm is required in front of and behind the hanging mechanism because the ceiling-hole width is $-15 \leq x \leq 15$.

B. Hanging-Mechanism Design

There are five hanging-mechanism requirement specifications as follows:
  i) support of 50 kg without unintentional release under loading;
  ii) single-action switching between lock and release states (insertion or extraction, Section II-C);
  iii) maximum $S = 15$ mm and minimum $C = 5$ mm (see Section III-A);
  iv) ease of incorporation with the crawler mechanism;
  v) insertion and locking capability for ceiling hole with shape isotropic to the two orthogonal directions (because the robot moves in the two orthogonal directions).

Further, a significant constraint condition for industrial application is minimization of the actuator number.

Hence, we designed three locking mechanisms: A) cam; B) plunger; and C) twist lock (see Fig. 14). To reduce the motions of each mechanism, we also designed four switching mechanisms: α) push–pull; β) push lock; γ) knock; and δ) guide (see Fig. 15). Here, α) achieves switching of the lock and release states when a rod is pulled up and down. Further, β) can lock via insertion and release achieved by pulling a switching rod, like the push–pull mechanism. The γ) mechanism switches states only through pushing, like the action of a ballpoint pen. The pushing motion switches between the Step 2) upper and Step 4) lower positions. Finally, the δ) mechanism achieves switching of two rotational states through sliding and pushing of a guide and cam, respectively. We designed a ceiling hole for insertion and restraint of each locking mechanism, with an isotropic shape
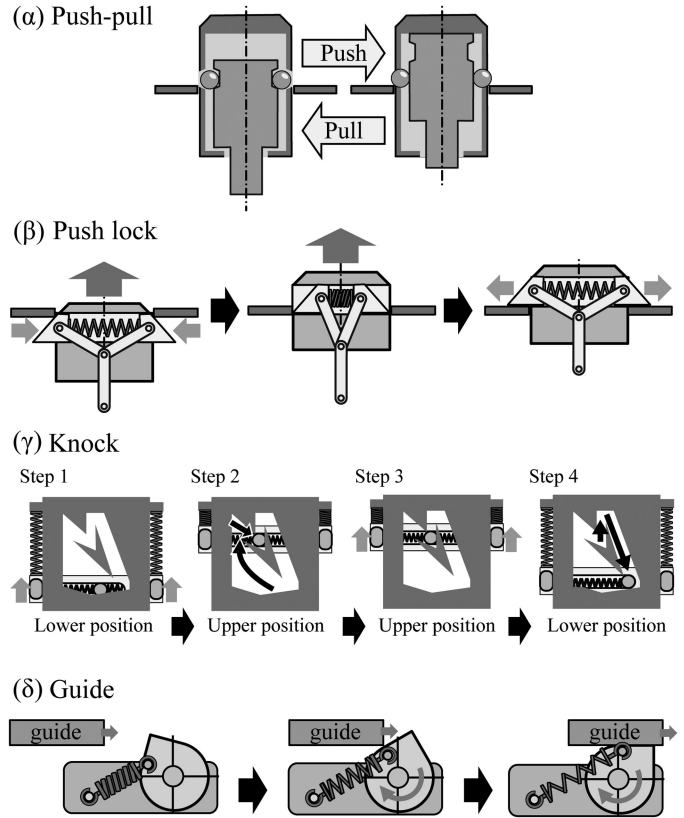

Fig. 15.   Conceptual sketches of state transition mechanisms.
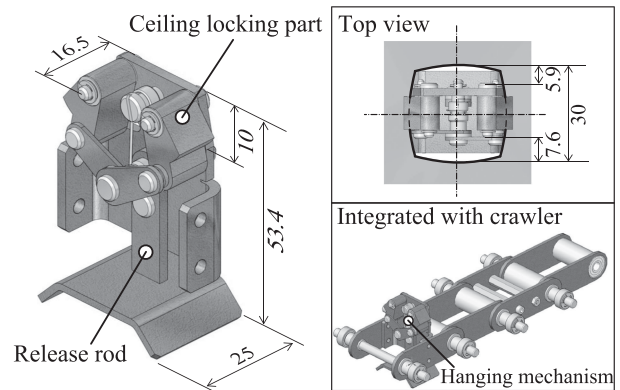

Fig. 16.   Overview of hanging mechanism.

for the traveling direction and the minimum width. We then compared five design proposals, excluding combinations that could not be realized or that were obviously inferior to other combinations (see Table II). The A) + β) combination exhibited the required S and C, with only one action at insertion and extraction. Locking and release could be performed with the same actuator. Therefore, we adopted the cam + push lock method as the hanging mechanism.

Hence, we designed the hanging mechanism shown in Fig. 16; the push stroke was 10 mm and C was 5.9 mm. The ceiling-hole width was set to 30 mm and the hole was square with four sides inflated, as shown in the top view of Fig. 16. This design

TABLE II
COMPARISON OF HANGING-MECHANISM CANDIDATES

Required specifications	(A) Cam		(B) Plunger		(C) Twist lock
	(β) Push lock	(γ) Knock	(α) Push-pull	(γ) Knock	(δ) Guide
Hanging stroke less than 15 mm	✓	✓	×	✓	✓
Hanging clearance exceeding 5 mm	✓	×	×	×	×
One action type for lock process	✓	✓	×	✓	×
One action type for release process	✓	×	×	×	×
Same actuator for locking & release processes	✓	×	×	×	✓

Fig. 17. Hanging-mechanism movement.

Fig. 18. Stress analysis model of hanging mechanism during locking.
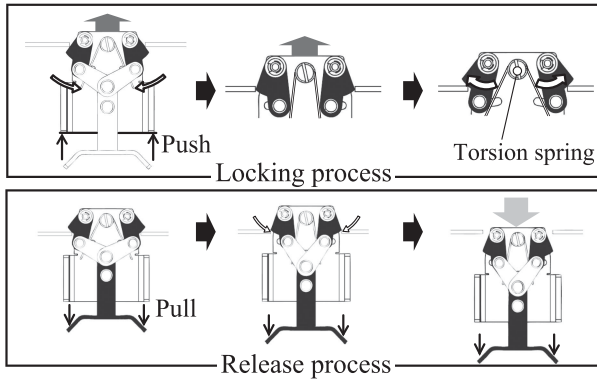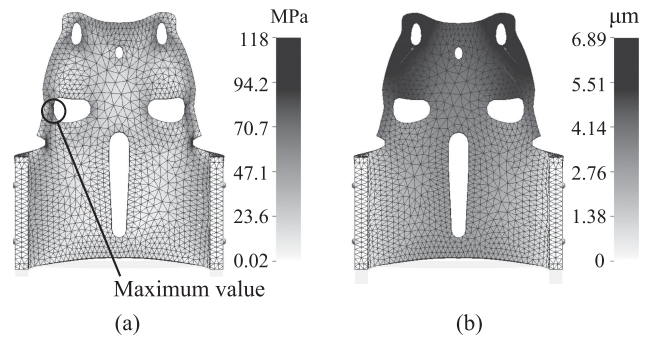

Fig. 19. Results obtained for (a) von Mises stress and (b) displacement.

targeted a centering function that reduces hanging-mechanism displacement.

Fig. 17 shows the behavior of the hanging mechanism during locking and release. During locking, the hanging mechanism is pushed upward and the locking part touches the ceiling hole. The locking part is inserted while closing by receiving force from the ceiling hole. When it is inserted with a pushing stroke, the locking part opens via a torsion spring and locks into the ceiling hole. During release, the locking part closes by pulling the release rod of the hanging mechanism. Further pulling extracts it from the ceiling hole. Thus, the locking and release operations are conducted via push and pull motions during insertion and release, respectively.

A stress analysis using the finite-element method (FEM) was performed to evaluate the strength of the hanging mechanism during locking. The applied load was $\omega = 100$ kg, and the load $P = \omega/2 \sin 40°$ was applied to a single ceiling locking part. The base plate is made of 2.3-mm cold-rolled steel sheet with a yield stress of 160 MPa. In the FEM stress analysis, the load P pushes the two holes of the plate and both the side surfaces of the plate constrain it, as shown in Fig. 18. Fig. 19 shows the stress analysis result. The maximum value of the von Mises stress 118 MPa (in a circle) is less than the yield stress of 160 MPa. This indicates that the base plate satisfies the strength requirement. Consequently, the hanging mechanism can support a large payload of more than 100 kg. This means that a single locked hanging mechanism
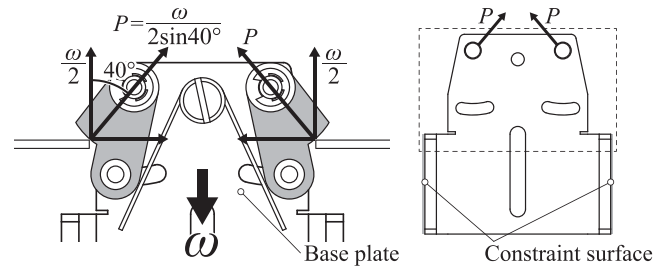
provides enough adhesion force to keep the robot hanging from the ceiling and preventing it from falling.

Hence, the hanging mechanism can lock onto the ceiling hole by simply pushing into the hole along the guide described in Section III-A. For extraction from the ceiling hole, a mechanism for pulling the releasing rod is required. When this mechanism is designed with a guide, etc., and without actuators, the guide shape must transform according to the traveling direction, which complicates the mechanism. Therefore, in the proposed design, an actuator is used for the pulling mechanism and switching is performed according to the traveling direction. Fig. 20 shows the push–pull mechanism, which employs a compact linear actuator (Oriental Motor Co., "DRL28G-03A1PN-KD"). By also using the latter as a pushing mechanism during hanging-mechanism insertion, insertion corresponding to the deflection of the ceiling surface and robot body is possible.
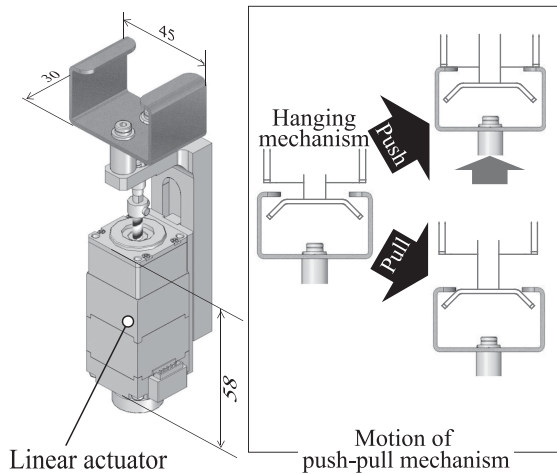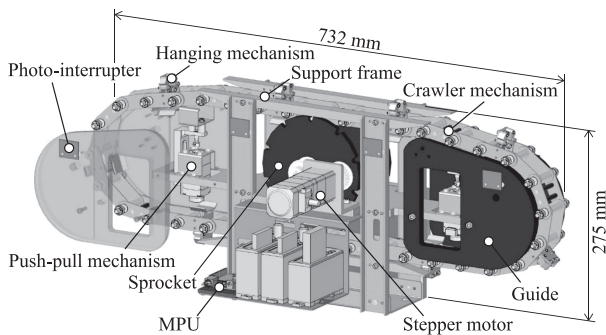
Fig. 20.   Overview of push–pull mechanism.

Fig. 21.   Overview of linear mobile robot.

C. Integration Into Linear Mobile Robot

Fig. 21 shows the designed linear mobile robot integrating the abovementioned mechanisms. Sprockets engage with the crawler link axles and rotate the crawler, which is driven by a stepper motor. In accordance with the approach suggested in Section II-B, the transport load is supported only by hanging mechanisms in contact with the support frame fixed to the main frame. Therefore, the load is not applied to the hanging mechanism operated by the push–pull mechanism. The hanging-mechanism positions on the crawler mechanism are recognized by the photointerrupter, and the position data are used for timing calculation of the push–pull mechanism. The necessary time for pulling motion is approximately 0.4 s, and this time has positive and negative margin times because the push–pull mechanism can either push or pull the hanging mechanism with a margin of 20 mm in the front to rear direction. Hence, the linear mobile robot can push and pull the hanging mechanisms without deceleration of its linear movement. During insertion, the robot can realize the hanging-mechanism insertion flow shown in Fig. 22 at a constant speed. When the hanging mechanism moves along the guide, photointerrupters recognize the positions, and the push–pull mechanism pushes at the times calculated from the recognized positions.
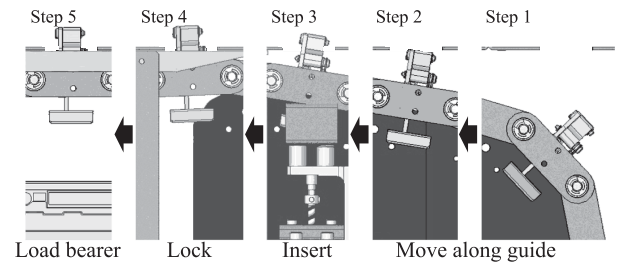

Fig. 22.   Hanging-mechanism insertion process flow.

D. Turning Mechanism Design

There are two requirements for the turning mechanism at the turntable guide proposed in Section II-E: 1) a turntable lock–unlock function and 2) a turning angle correction function after the turning motion. In addition, each function should be realized without actuators on the ceiling.

For the robot to enter the accurately positioned turntable, two functions are necessary—rotation locking when the robot is absent and unlocking at initiation of the robot turning motion. We propose a locking mechanism using permanent magnets and pins. Fig. 23 shows the turning process flow. The locking and unlocking functions are shown at the bottom of the figure.

Step 1) The robot enters the turntable, at which time a lock claw locks the turntable.

Step 2) The robot stops at the center of turntable after entry.

Step 3) When the robot rotates a rotating arm with an actuator to the prescribed position, attracted metal attached to the rotating-arm tip attaches to a permanent magnet on the ceiling. The attracted metal simultaneously raises an unlock pin attached to the lock claw and unlocks the turntable.

Step 4) The robot rotates the rotating arm and body together with the turntable. If the magnet adsorption force is designed to be sufficiently larger than the rotational frictional force of the turntable, the rotating arm can rotate the robot without detaching from the magnet.

Step 5) When the robot exits from the turntable, the rotating arm separates from the permanent magnet and the lock claw falls to lock the turntable again.

Thus, the lock–unlock and turning functions are realized by the single actuator of the rotating arm. Fig. 24 shows the designed turntable and lock mechanism and Fig. 25 shows HanGrawler integrated with the rotating arm and linear mobile robot. The dimensions of the HanGrawler are 732 mm wide, 713 mm deep, and 535 mm high. The weight of the device is 18 kg, and there are four actuators in the device. A servomotor (Futaba Co., RS405CB) is used for the rotating arm. As discussed in Section II-E, the actuator is mounted on the robot side only. Considering servomotor backlash and rotating-arm deflection, a mechanism for correcting the turntable angle after turning is installed on the table (see Fig. 24). The mechanism has an index plate and a plunger. The plunger has a roller which is pushed by an internal spring. By pressing the plunger into the valley of
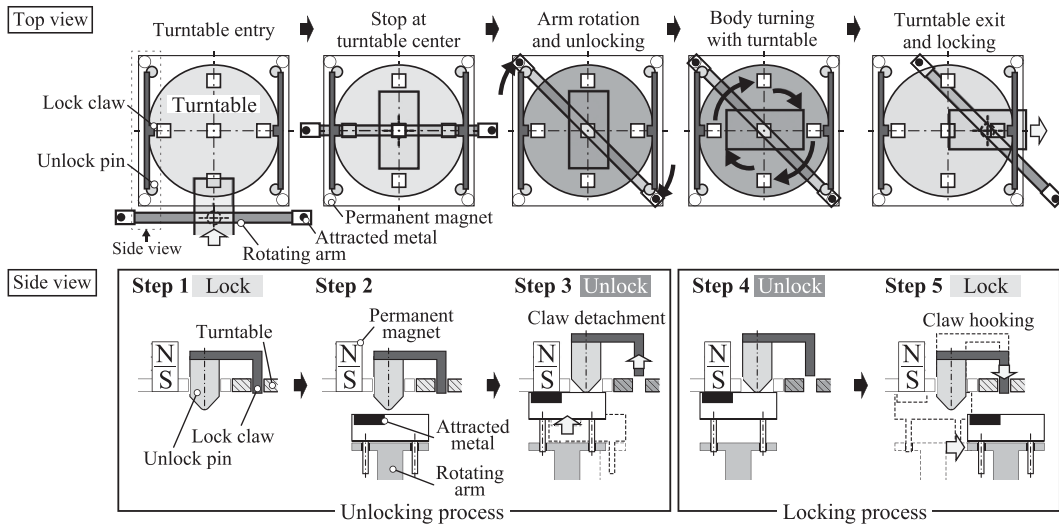
Fig. 23. Conceptual diagram of turning process and lock–unlock process flow.
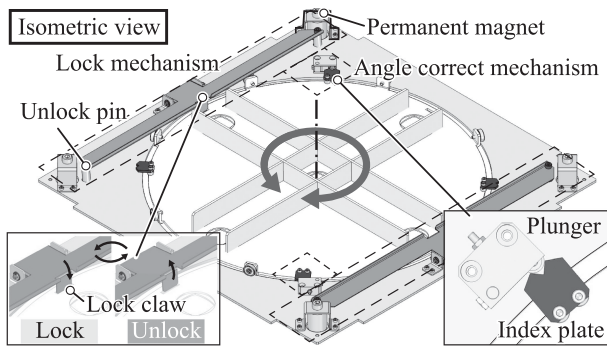

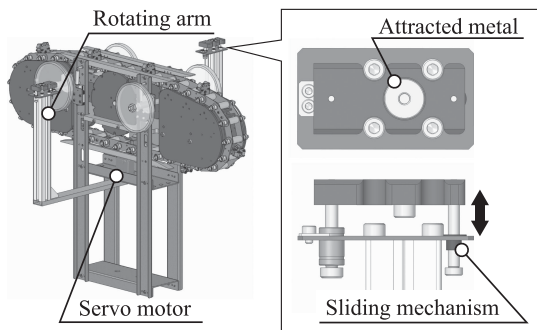Fig. 24. Overview of turntable mechanism.

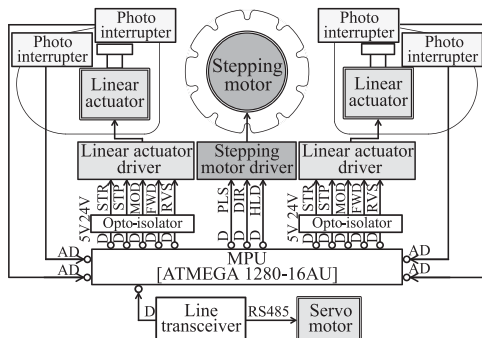Fig. 25. Overview of HanGrawler.

Fig. 26. Functional block diagram of electrical system.
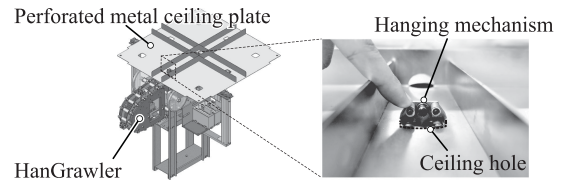

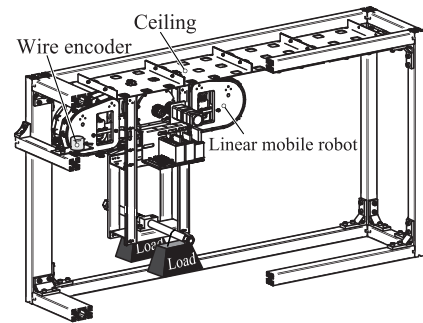Fig. 27. Snapshot of hanging mechanism inserted into ceiling hole.

Fig. 28. Overview of experimental device.
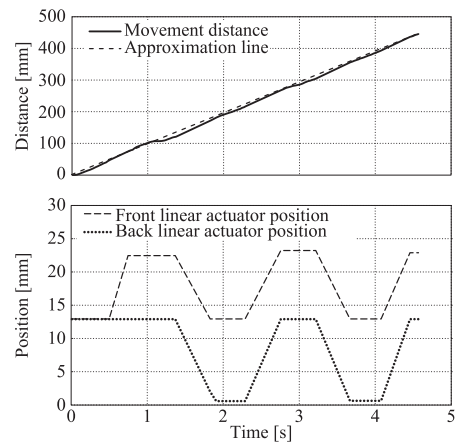

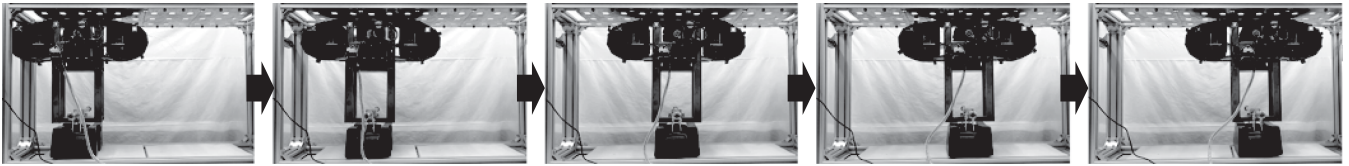Fig. 29. Measured data example (load: 60 kg).

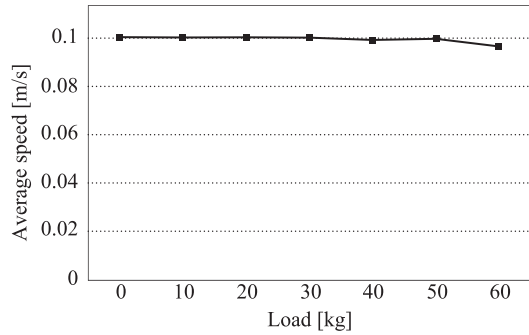Fig. 30.   Sequential snapshots of linear mobile robot locomotion.

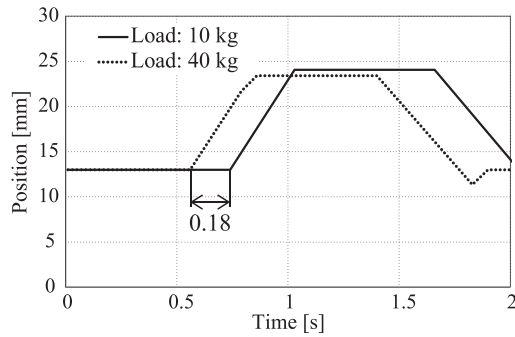Fig. 31.   Average movement speed of each load.

Fig. 32.   Comparison of front linear actuator position for 10- and 40-kg loads.

Fig. 33.   Overview of experimental device for turning experiment.
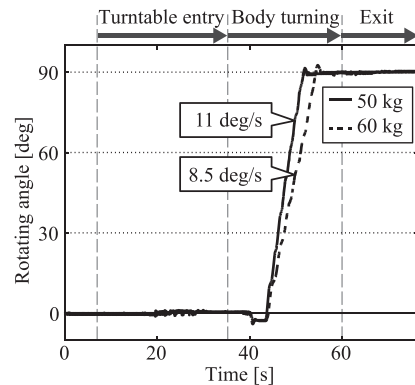
Fig. 34.   Measured data example (load: 50, 60 kg) for comparison of angular velocity.

the index plate, it is possible to correct and hold the turntable turning angle without any sensors. There is also a function to hold the table angle when the robot exits the turntable, which is in the unlocked state. Hence, a turning operation with high angular reproducibility is realized.

E. Electrical System

Fig. 26 shows a functional block diagram of the HanGrawler electrical system. Actuator control and hanging-mechanism position recognition are performed by an 8-b microcontroller (Atmel Co., ATmega2560).

IV. MOVEMENT PERFORMANCE EVALUATION EXPERIMENT

A. Hanging Experiment

We verified the stability of the hanging ability on the perforated metal ceiling plate. Fig. 27 shows the hanging mechanism of the HanGrawler. When this mechanism is locked and a load is applied, the entire mechanism is intended to be located at

the center of the hole and to be solidly anchored to the ceiling hole. A regularly locked hanging mechanism has sufficient load durability, and the influence of any external interference is quite low.

B. Linear Movement Performance Evaluation Experiment

We evaluated the performance of the linear mobile robot and verified that ceiling movement is possible in combination with mechanical hanging and the crawler mechanism, and that the target load of 50 kg and 0.1-m/s carrying speed are achievable. Fig. 28 shows the experiment device. The experiment settings were as follows: Load: 0, 10, 20, 30, 40, 50, 60 kg (three times each) and movement distance: More than 400 mm in the horizontal direction. To measure the movement distance, a wire-type linear scale (Microtech Laboratory Inc., MLS-30-4500-1000) was used. To measure the linear-actuator pushing position, the microcontroller command value history was used.

| Enter turntable | Rotate arm | Turn body | Finish turning 90° | Leave turntable |

Fig. 35. Sequential snapshots of HanGrawler turning.

Figs. 29 and 30 show sample data acquired in this experiment and the snapshots of the linear mobile robot movement, respectively. The robot movement was close to uniform speed; thus, continuous movement was achieved. Fig. 31 shows the relationship between the load and average movement speed. The load influence was small and the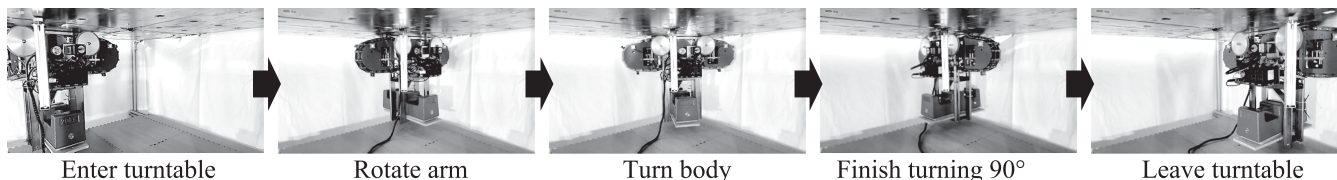 robot could move at a constant speed of 0.1 m/s, regardless of the load. Thus, we achieved continuous movement on the ceiling and both the target load and loaded speed of 50 kg and 0.1 m/s for the developed robot.

The push timing of the hanging mechanism was confirmed to deviate with increased supporting load. Fig. 32 compares the linear actuator positions during the push operation when the supporting loads were 10 and 40 kg. Ceiling movement was possible by adjusting the push timing between loads of 0, 10, and 20 kg and loads of 30, 40, 50, and 60 kg. As shown in Fig. 32, the push timing was shifted by 0.18 s. We believe the timing shift is needed because of ceiling deflection due to the increase in the required push distance according to the load.

C. Turning Experiment

With regard to HanGrawler and the turntable, we verified the feasibility of the turning motion, lock mechanism, and angle-correction mechanism. Fig. 33 shows the experiment device. HanGrawler moved as shown by the arrow, traveling straight, turning 90° to the right, and then, proceeding straight. The experiment settings were as follows: Load: 0, 10, 20, 30, 40, 50, 60 kg (three times each) and turning angle: 90° (right). Motion capture (NaturalPoint Inc., Prime17 W) was used for measurement.

Figs. 34 and 35 show an example of the acquired data and the turning movement, respectively. The time period for HanGrawler entry to the turntable was up to 35 s, with body turning proceeding until 60 s. Then, HanGrawler left the turntable. Thus, HanGrawler turned 90° using the turning mechanism at a constant angular velocity of 11°/s with a load of 50 kg. Even for a 60-kg load, turning was achieved with an angular velocity reduction to 8.5°/s. We believe that the moment of inertia increased with the loading; then, the servomotor torque was insufficient.

Through these experiments, HanGrawler demonstrates high stability and does not fall away from the ceiling. When the push timing is inadequate and the hanging mechanism is jammed against the ceiling holes, HanGrawler stops moving. Even in this case, HanGrawler continues to hang from the ceiling; thus, it is evident that HanGrawler has a high level of stability.

V. Conclusion

To realize a ceiling mobile transport device with easy route adjustment, we developed a mechanical hanging mechanism for ceiling-plate attachment and a crawler mechanism for continuous movement. As the mechanical hanging and crawler mechanisms have not been implemented previously, we clarified the problem and proposed solutions by designing devices based on these solutions. In this article, we proposed a design method to draw the ceiling-hole trajectory with respect to the hanging mechanism and showed that a guide shape combining a straight line and an arc is important for a realistic solution. In the experiment, we succeeded with a transportation load of 60 kg and speed of 0.1 m/s regardless of load, and demonstrated the feasibility of the proposed method. This clarified the design solution for the ceiling mobile robot combining the mechanical hanging and crawler mechanisms. The crawler-and-hanging mechanism realized high-speed continuous movement with a heavy load, which has been impossible with ceiling mobile robots designed to date.

By arranging a support frame between the ceiling and hanging mechanism, the load on the hanging mechanism could be eliminated during locking and release. Further, a small power actuator could be used as the lock and release actuator, separately from those of previous works. In addition, by limiting the number of locking and release actions to only one, the time required for the actions was shortened and 0.1-m/s ceiling movement was realized. The proposed turning mechanism allowed 2-D motion of the linear mobile robot. For the combination of the turntable and robot-driven mechanism, mounting the actuator on the robot only successfully suppressed the number of actuators in the robot group and along the entire ceiling at the production site. This approach should also facilitate ceiling recombination during line changing. In the future, it will be necessary to develop an optimal route design method for production sites using this system and to further accelerate the movement mechanism under the same loading conditions.

References

[1] I. F. A. Vis, "Survey of research in the design and control of automated guided vehicle systems," *Eur. J. Oper. Res.*, vol. 170, no. 1, pp. 677–709, May 2006.

[2] G. Ullrich, *Automated Guided Vehicle Systems: A Primer with Practical Applications*. Berlin, Germany: Springer-Verlag, 2015.

[3] S. Hirose, A. Nagakubo, and R. Toyama, "Machine that can walk and climb on floors, walls and ceilings," in *Proc. 5th Int. Conf. Adv. Robot., Robots Unstruct. Environ.*, Pisa, Italy, 1991, vol. 1, pp. 753–758.

[4] Q. Hong, R. Liu, H. Yang, and X. Zhai, "Wall climbing robot enabled by a novel and robust vibration suction technology," in *Proc. Int. Conf. Autom. Logistics*, Shenyang, China, 2009, pp. 331–336.

[5] I.-M. Chen and S. H. Yeo, "Locomotion of a two-dimensional walking-climbing robot using a closed-loop mechanism: From gait generation to navigation," *Int. J. Robot. Res.*, vol. 22, no. 1, pp. 21–40, 2003.

[6] J. Xiao, J. Z. Xiao, N. Xi, R. L. Tummala, and R. Mukherjee, "Fuzzy controller for wall-climbing microrobots," *IEEE Trans. Fuzzy Syst.*, vol. 12, no. 4, pp. 466–480, Aug. 2004.

[7] Y. Yoshida and S. Ma, "A wall-climbing robot without any active suction mechanisms," in *Proc. IEEE Int. Conf. Robot. Biomimetics*, Phuket, Thailand, 2011, pp. 2014–2019.

[8] T. T. Tun, M. R. Elara, M. Kalimuthu, and A. Vengadesh, "Glass facade cleaning robot with passive suction cups and self-locking trapezoidal lead screw drive," *Autom. Construction*, vol. 96, pp. 180–188, Dec. 2018.

[9] M. Fujita, S. Ikeda, T. Fujimoto, T. Shimizu, S. Ikemoto, and T. Miyamoto, "Development of universal vacuum gripper for wall-climbing robot," *Adv. Robot.*, vol. 32, no. 6, pp. 283–296, Apr. 2018.

[10] J. Xiao, B. Li, K. Ushiroda, and Q. Song, "Rise-rover: A wall-climbing robot with high reliability and load-carrying capacity," in *Proc. IEEE Int. Conf. Robot. Biomimetics*, Zuhai, China, 2015, pp. 2072–2077.

[11] Y. K. Song, C. M. Lee, I. M. Koo, D. T. Tran, H. Moon, and H. R. Choi, "Development of wall climbing robotic system for inspection purpose," in *Proc. IEEE/RSJ Int. Conf. Intell. Robots Syst.*, Nice, France, 2008, pp. 1990–1995.

[12] J. Grieco, M. Prieto, M. Armada, and P. de Santos, "A six-legged climbing robot for high payloads," in *Proc. IEEE Int. Conf. Control Appl.*, Trieste, Italy, 1998, vol. 1, pp. 446–450.

[13] P. Kriengkomol, K. Kamiyama, M. Kojima, M. Horade, Y. Mae, and T. Arai, "New tripod walking method for legged inspection robot," in *Proc. IEEE Int. Conf. Mechatron. Autom.*, Harbin, China, 2016, pp. 1078–1083.

[14] T. Bandyopadhyay *et al.*, "Magneto: A versatile multi-limbed inspection robot," in *Proc. IEEE/RSJ Int. Conf. Intell. Robots Syst.*, Madrid, Spain, 2018, pp. 2253–2260.

[15] T. Sato, R. Fukui, H. Morishita, and T. Mori, "Construction of ceiling adsorbed mobile robots platform utilizing permanent magnet inductive traction method," in *Proc. IEEE/RSJ Int. Conf. Intell. Robots Syst.*, Sendai, Japan, 2004, pp. 552–558.

[16] L. Kalra, J. Gu, and M. Meng, "A wall climbing robot for oil tank inspection," in *Proc. IEEE Int. Conf. Robot. Biomimetics*, Kunming, China, 2006, pp. 1523–1528.

[17] G. Lee, G. Wu, S. H. Kim, J. Kim, and T. W. Seo, "Combot: Compliant climbing robotic platform with transitioning capability and payload capacity," in *Proc. IEEE Int. Conf. Robot. Autom.*, Saint Paul, MN, USA, 2012, pp. 2732–2742.

[18] M. Tavakoli, J. Loureno, C. Viegas, P. Neto, and A. T. de Almeida, "The hybrid omniclimber robot: Wheel based climbing, arm based plane transition, and switchable magnet adhesion," *Mechatronics*, vol. 36, pp. 136–146, Jun. 2016.

[19] F. Howlader, M. D. Omar, and T. P. Sattar, "Novel adhesion mechanism and design parameters for concrete wall-climbing robot," in *Proc. SAI IntelliSys*, London, U.K., 2015, pp. 267–273.

[20] O. Kermorgant, "A magnetic climbing robot to perform autonomous welding in the shipbuilding industry," *Robot. Comput. Integr. Manuf.*, vol. 53, pp. 178–186, Oct. 2018.

[21] G. D. Wile *et al.*, "Screenbot: Walking inverted using distributed inward gripping," in *Proc. IEEE/RSJ Int. Conf. Intell. Robots Syst.*, Nice, France, 2008, pp. 1513–1518.

[22] Y. Liu, S. Sun, X. Wu, and T. Mei, "A wheeled wall-climbing robot with bio-inspired spine mechanisms," *J. Bionic Eng.*, vol. 12, no. 1, pp. 17–28, Jan. 2015.

[23] F. Xu, B. Wang, J. Shen, J. Hu, and G. Jiang, "Design and realization of the claw gripper system of a climbing robot," *J. Intell. Robot Syst.*, vol. 89, no. 3/4, pp. 301–317, Mar. 2018.

[24] W. K. Chung, J. Li, Y. Chen, and Y. Xu, "A novel design of movable gripper for non-enclosable truss climbing," in *Proc. IEEE Int. Conf. Robot. Autom.*, Shanghai, China, 2011, pp. 519–525.

[25] "Machine tending robots," FANUC Co., Oshino, Japan. Accessed: Sep. 19, 2019. [Online]. Available: https://www.fanucamerica.com/industrial-solutions/manufacturi ng-applications/machine-tending-robots

[26] T. Satooka, H. Yamazoe, and J.-H. Lee, "Barb based fast movement of mobile module for deploying devices in reconfigurable intelligent space," in *Proc. IEEE 15th Int. Conf. Ubiquitous Robots*, Honolulu, HI, USA, 2018, vol. 2, pp. 622–627.

[27] R. Fukui, H. Morishita, T. Mori, and T. Sato, "Hangbot: A ceiling mobile robot with robust locomotion under a large payload (key mechanisms integration and performance experiments)," in *Proc. IEEE Int. Conf. Robot. Autom.*, Shanghai, China, 2011, pp. 4601–4607.

[28] L. Wang, L. Graber, and F. Iida, "Large-payload climbing in complex vertical environments using thermoplastic adhesive bonds," *IEEE Trans. Robot.*, vol. 29, no. 4, pp. 863–874, Apr. 2013.

[29] R. Chen, R. Liu, and H. Shen, "Design of a double-tracked wall climbing robot based on electrostatic adhesion mechanism," in *Proc. IEEE Workshop Adv. Robot. Social Impacts*, Tokyo, Japan, 2013, pp. 212–217.

[30] S. Kim, M. Spenko, S. Trujillo, B. Heyneman, V. Mattoli, and M. R. Cutkosky, "Whole body adhesion: Hierarchical, directional and distributed control of adhesive forces for a climbing robot," in *Proc. IEEE Int. Conf. Robot. Autom.*, Roma, Italy, 2007, pp. 1268–1273.

[31] M. P. Murphy, C. Kute, Y. Meng, and M. Sitti, "Waalbot II: Adhesion recovery and improved performance of a climbing robot using fibrillar adhesives," *Int. J. Robot. Res.*, vol. 30, no. 1, pp. 118–133, Jan. 2011.

[32] H. Wang and A. Yamamoto, "Analyses and solutions for the buckling of thin and flexible electrostatic inchworm climbing robots," *IEEE Trans. Robot.*, vol. 33, no. 4, pp. 889–900, Aug. 2017.

[33] Z. Yu, Y. Shi, J. Xie, S. X. Yang, and Z. Dai, "Design and analysis of a bionic adhesive foot for gecko robot climbing the ceiling," *Int. J. Robot. Autom.*, vol. 33, no. 4, pp. 445–454, Jul. 2018.

[34] "Forward running type—Automated guided vehicles," HEADS Co., Ltd., Miyako, Japan. Accessed on: Mar. 6, 2019. [Online]. Available: https://headscorp.co.jp/en/agv/pop_f2.html?8

[35] Y. Monden, *TOYOTA Production System: An Integrated Approach to Just-In-Time*, 4th ed. Boca Raton, FL, USA: CRC Press, 2011.

Rui Fukui (Member, IEEE) received the B.Eng. and M.Eng. degrees and the Ph.D. degree in information science and technology from the University of Tokyo (UTokyo), Tokyo, Japan, in 2002, 2004, and 2009, respectively.

From 2004 to 2006, he was an Engineer with the Special Vehicle Designing Section, Mitsubishi Heavy Industries, Ltd., Tokyo. From 2009 to 2013, he was a (Project) Assistant Professor with the Department of Mechano-Informatics, UTokyo. From 2013 to 2016, he was an Assistant Professor (Full-Time Lecturer) with the Department of Mechanical Engineering, UTokyo. Since 2016, he has been an Associate Professor with the Department of Human and Engineered Environmental Studies, Graduate School of Frontier Sciences, UTokyo. His research interests include human symbiotic robot system and mechanism design.

Dr. Fukui is a member of the Robotics Society of Japan.

Yudai Yamada (Student Member, IEEE) received the B.Eng. degree in mechanical engineering in 2018 from the University of Tokyo (UTokyo), Tokyo, Japan, where he has been working toward the M.Environ. degree in human environment informatics with the Department of Human and Engineered Environment Studies, Graduate School of Frontier Science, since 2018.

Mr. Yamada is a member of the Japan Society of Mechanical Engineers (JSME).

Keisuke Mitsudome received the B.Eng. degree in mechanical engineering in 2017 from the University of Tokyo (UTokyo), Tokyo, Japan, where he has been working toward the M.Environ. degree in human environment informatics with the Department of Human and Engineered Environment Studies, Graduate School of Frontier Science, since 2017.

Katsuya Sano received the B.Eng. and M.Eng. degrees in mechanical engineering from the University of Tokyo (UTokyo), Tokyo, Japan, in 2016 and 2018, respectively.

Since 2018, he has been an Engineer with Kawasaki Heavy Industries Motorcycle and Engine Company, Kawasaki Heavy Industries, Ltd., Tokyo, Japan.

Shin'ichi Warisawa received the B.Eng. and M.Eng. degrees and the Ph.D. degree in engineering from the University of Tokyo (UTokyo), Tokyo, Japan, in 1989, 1991, and 1994, respectively.

From 1994 to 2000, he was a Research Associate with the Precision and Intelligence Laboratory, Tokyo Institute of Technology, Tokyo, Japan. From 2000 to 2003, he was a Lecturer with the School of Engineering, UTokyo and an Associate Professor from 2003 to 2010. From 2010 to 2011, he was a Visiting Scholar with the Massachusetts Institute of Technology, Cambridge, MA, USA. From 2012 to 2015, he was an Associate Professor with the Graduate School of Frontier Science, UTokyo. Since 2015, he has been a Professor with the Department of Human and Engineered Environmental Studies, Graduate School of Frontier Sciences, UTokyo.

Prof. Warisawa is a member of the Japan Society of Mechanical Engineers (JSME), the Robotics Society of Japan (RSJ), and the Japan Society for Precision Engineering (JSPE).